JOURNAL OF MATERIALS SCIENCE 28 (1993) 3635–3644

Acoustic microscopy of ceramic-fibre composites

Part I *Glass-matrix composites*

C. W. LAWRENCE, G. A. D. BRIGGS
Department of Materials, University of Oxford, Parks Road, Oxford, OX1 3PH, UK
C. B. SCRUBY, J. R. R. DAVIES
AEA Technology, Harwell Laboratory, Didcot, Oxon, OX11 0RA, UK

The microstructure of Nicalon-reinforced borosilicate glass was studied using scanning acoustic microscopy (SAM) and scanning electron microscopy (SEM). Acoustic micrographs exhibited high contrast, and the formation of Rayleigh-wave-interference fringes both within and around fibres allowed the *in-situ*-fibre and matrix elastic moduli to be estimated. The matrix was found to have undergone partial devitrification resulting in the formation of cristobalite. The presence of a high volume fraction of reinforcing fibres was found to have little effect on cristobalite formation and distribution. The thermal expansion mismatch between β-cristobalite and the devitrified glass matrix and the β/α-cristobalite phase change were found to give rise to extensive microcracking around individual cristobalite grains and partial fibre/matrix debonding.

1. Introduction

Whilst exhibiting excellent thermal properties coupled with low density, a high elastic modulus and reasonable mechanical strength, conventional engineering ceramics exhibit poor fracture toughness. In the early 1970s it was found that the addition of 0.40 volume fraction of carbon fibres to borosilicate (Pyrex) glass increased its work of fracture from $10\,\mathrm{J\,m^{-2}}$ to $3.7\,\mathrm{kJ\,m^{-2}}$ [1]. The subsequent development of small diameter ($< 20\,\mu\mathrm{m}$) silicon oxycarbide fibres such as Nicalon and Tyranno has permitted the fabrication of ceramic-matrix composites (CMCs) with fracture toughnesses approaching those of metals. Thus the addition of 0.49 volume fraction, V_f, of Nicalon fibres to borosilicate glass produces a CMC with a work of fracture of $50\,\mathrm{kJ\,m^{-2}}$ [2]. This increase in work of fracture is primarily due to the low interfacial frictional shear strength (IFSS) between the fibres and matrix, allowing broken fibres to be pulled out of the matrix [3].

The full potential of this type of material is not often achieved because of the three following reasons.

1. Fibre properties are lost due to aggressive processing conditions, e.g. at temperatures of ~ 1000 °C,
2. Inappropriate microstructures are generated during composite fabrication. If a significant difference in the coefficient of thermal expansion (CTE) exists between the matrix and the fibre reinforcement then large residual thermal stresses can exist in the composite at room temperature, which may exceed the matrix fracture stress and hence give rise to spontaneous matrix microcracking,
3. Matrix microcracking occurs around fibres at relatively low stresses which allows environmental ingress and loss of composite properties.

Problems 1 and 2 can be solved by careful optimization of microstructures during fabrication in order to tailor fibre, matrix and fibre/matrix interfacial properties. Matrix microcracking under stress is the principal obstacle to the use of CMCs. At high temperatures access of the environment to the fibres [4] causes their fracture, and the strength of the material is therefore limited to the matrix microcracking stress.

Defects such as matrix microcracks generated during fabrication or use are difficult to detect in CMCs using optical microscopy (OM) due to their small dimensions. In back-scattered scanning electron microscopy (SEM), the low atomic numbers of the composite constituents give rise to poor contrast. In addition, since most ceramics are poor electrical conductors, CMCs normally have to be carbon or gold coated to obtain a clear image.

Scanning acoustic microscopy (SAM) has been shown to be highly sensitive to the presence of cracks and elastic discontinuities in monolithic ceramics and metals [5–7]. The contrast in SAM is directly related to the elastic properties of the surface being examined. This allows the discrimination of optically transparent phases and the imaging of extremely fine surface cracks and pores via the mechanism of Rayleigh-wave-fringe formation [8], with a theoretical resolution limit of approximately 10 nm [9]. The surface of the specimen does not need to be etched in order to enhance contrast from second phases.

2. Experimental procedure

The material examined in the current work was borosilicate glass reinforced with Nicalon-silicon-oxycarbide fibres, fabricated at the Harwell Laboratory [2]. The material was fabricated by hot pressing at 950 °C and 10 MPa for 10 min, to give optimum mechanical properties. The reinforcing fibres were arranged uniaxially, with a nominal fibre volume fraction of 0.45. In order to investigate the effect of fibre volume fraction on composite microstructure, a specimen containing a single reinforcing fibre (i.e. effectively a zero fibre volume fraction) was fabricated under identical conditions. Typical properties which have been reported for this composite system are shown in Table I along with the equivalent properties for the borosilicate-glass matrix and Nicalon fibres.

Acoustic microscopy requires samples to be flatter than the acoustic wavelength in water at the frequency used (1.9 GHz for the current work) in order to minimize spurious phase contrast. To ensure an adequate surface for examination of the composite, the following procedure was used. Samples of composite (typical dimensions $2 \times 10 \times 5$ mm) were cut from the as-pressed composite coupon using a thin-bladed annular diamond saw. Samples were then vacuum embedded in an epoxy resin so that the composite presented a transverse section to the surface. Once the epoxy was fully cured, the sample was attached to a precision polishing jig and progressively lapped and polished using in turn 6, 1, 0.25 and 0.1 μm diamond pastes with a silicone-oil lubricant on scrolled brass platens, at low loads. Napless cloths were found to give relief between fibres and matrix, giving rise to spurious contrast in the acoustic microscope, although these cloths give an adequate finish for optical microscopy. Indeed, for examination by SEM using secondary-electron imaging, it was found necessary to include an extra polishing stage (0.25 μm diamond paste on a napless cloth) in order to emphasize relief, and hence contrast, between microstructural constituents. The final polishing stage for acoustic microscopy involved the use of Syton (a colloidal silica solution with a 0.1 μm particle size) on a polyurethane-coated platen for 10 min to remove fine scratches and provide a mild etch of the glass matrix.

TABLE I Mechanical properties of uniaxial 7740/SiC and its constituents

Property	7740/SiC ($0.49\ V_f$)	7740 borosilicate glass	Nicalon SiC fibre
Young's modulus (GPa)	120[a]	63[b]	196[c]
Shear modulus (GPa)	51[d]	28[b]	77[e]
Tensile strength (MPa)	580[f]	48[b]	2750[c]
Work of fracture ($J\ m^{-2}$)	50 000[a]	10	–
CTE ($10^{-6}\ °C^{-1}$)		3.25[b] (25–300 °C)	1–2[c,g]
Density ($kg\ m^{-3}$)	2390[h]	2230[b]	2550[c]

[a] Dawson *et al.* [2].
[b] Chyung [10].
[c] Nippon Carbon Company [11].
[d] Seerat un Nabi and Derby [12].
[e] Grande *et al.* [13].
[f] Briggs and Davidge [14].
[g] Most researchers quote a value of $3.25 \times 10^{-6}\ °C^{-1}$ for 20–600 °C.
[h] Calculated assuming the rule of mixtures.

Specimens were examined using the following microscopes: an Olympus BHM optical microscope, a Leica SAM (hereafter ELSAM), a Hitachi S-530 scanning electron microscope with a secondary-electron detector, a Jeol JSM 35X in back-scattered mode, and a Cameca microprobe. Samples for SEM examination were carbon coated to prevent charge build-up on the specimen surface and to minimize beam damage to the composite. In addition a non-imaging acoustic microscope, a line-focus-beam microscope (LFBM), was used to obtain Rayleigh-wave velocities from bulk borosilicate glass and hot-pressed silicon carbide.

3. Results

3.1. Composite microstructure

OM was used to examine the basic composite microstructure. Fig. 1 shows an optical micrograph of Nicalon-reinforced borosilicate glass (7740/SiC). The fibre distribution can be seen to be comparatively poor, with clusters of fibres occurring. There is no indication of the arrangement of the fibres in the original tows. Only sporadic instances of open-surface porosity (approximately 0.001 area fraction) were visible, and they were invariably associated with matrix-denuded regions between close-packed fibres. The matrix consisted of a crystalline phase in an amorphous glass matrix, with microcracks just visible in the matrix linking adjacent fibres, the contrast from both being poor.

More detailed microstructural information was obtained on examining the composite by SAM. Fig. 2 shows a low-magnification acoustic micrograph of the 0.45 V_f composite. The crystalline matrix phase has high contrast with respect to both the glassy matrix phase and the silicon-carbide fibres. Cracks, delineated by Rayleigh-wave-interference fringes occur in both the glass and crystalline components of the

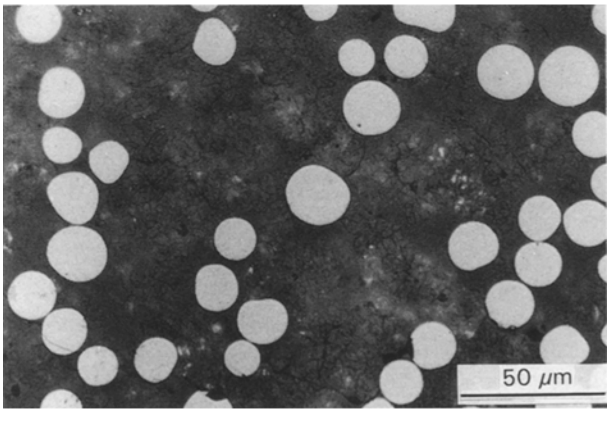

Figure 1 Optical micrograph of a 7740/SiC glass showing the general composite microstructure.

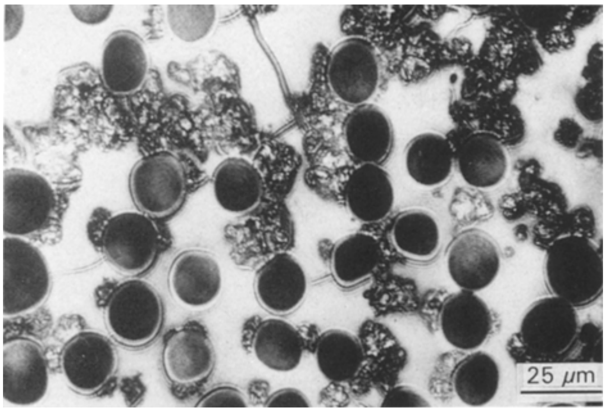

Figure 2 Scanning acoustic micrograph of a 7740/SiC glass taken at a defocus of $z = -2.8$ μm with an imaging frequency of 1.9 GHz. Note the strong contrast between fibres, matrix and microcracks.

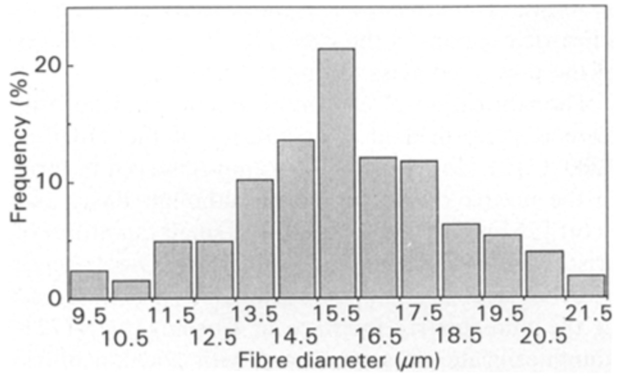

Figure 3 Histogram showing the measured fibre-diameter distribution of Nicalon fibres in a 7740/SiC glass. The mean = 15.7 μm, standard deviation = 2.6 μm and number of samples = 206.

matrix. The volume fraction of the latter was measured as 0.40 ± 0.05. The fibres deviate from their nominal circular cross-section and diameter. The mean fibre diameter measured from the electron micrographs was 15.7 μm, with an approximately normal distribution (Fig. 3) and a standard deviation of 2.6 μm.

Acoustic micrographs such as Fig. 2 all showed interference fringes within both the silicon-carbide fibres and the glass-matrix component. These fringes were visible at all values of defocus, z, but they were faint at focus. Fringes in the fibres have the same appearance as growth rings in trees. They are formed by interference between the normal component of an incident wave and the component reflected from the fibre–matrix interface, in a manner analogous to fringe formation from surface-breaking cracks oriented normally to the surface (Fig. 4). By carefully measuring the spacing of the Rayleigh fringes, δx, from high-magnification acoustic micrographs, the Rayleigh velocity, v_R, for the fibres can be calculated for a known imaging frequency. A mean Rayleigh velocity of 5320 m s^{-1} was calculated for the Nicalon-silicon-carbide fibres. This value is lower than the value of 6729 m s^{-1} for bulk hot-pressed silicon carbide as measured using the LFBM. The measured Rayleigh-wave velocity can then be used to calculate the shear modulus and Young's modulus of the material in which the fringes form (see Part II [15]).

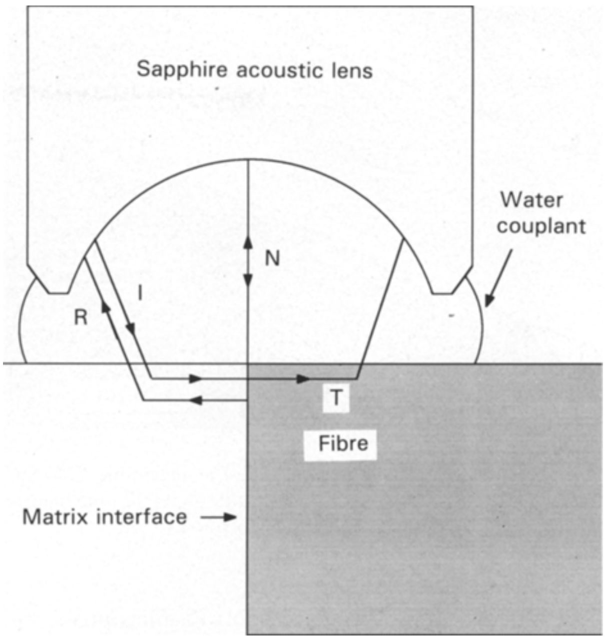

Figure 4 Schematic diagram of the mechanism of fringe formation in the matrix and fibres. I is the Rayleigh wave incident on the fibre/matrix, R the reflected wave component, and T the transmitted wave component. N is the normal component of the longitudinal waves in the water couplant incident on the surface of the composite. Note that the incident and reflected Rayleigh waves follow the same path.

Inserting the appropriate values yields an *in-situ* shear modulus of 89 GPa and a Young's modulus of 205 GPa for Nicalon-silicon-carbide fibres incorporated in a glass matrix. These are in good agreement with the manufacturer's quoted values [10] shown in Table I, but are slightly higher than values measured by independent researchers (see Part II [15]).

The Rayleigh-wave-interference fringes formed in the glass component of the matrix can, by the same process, be used to calculate the corresponding elastic properties of the glass. The measured Rayleigh-wave velocity of 3800 m s^{-1} yields a shear modulus of 39 GPa and a Young's modulus of 93 GPa. In comparison the Rayleigh-wave velocity of bulk borosilicate glass measured using the LFBM was 3324.2 m s^{-1}, giving a shear modulus of 29.7 GPa and a Young's modulus of 62.3 GPa, in good agreement with the data shown in Table I. As the borosilicate-glass matrix has undergone significant devitrification, some change in its elastic properties would be expected.

3.2. Matrix crystalline phase

The crystalline phase observed in the glass matrix has a granular "flowery" appearance with an individual grain (or "petal") size of 3–5 μm (Fig. 5). This phase was observed in both the 0.49 V_f composite specimen and the single fibre specimen. This phase resulted from devitrification of the borosilicate-glass matrix during fabrication of the composite. Chemical analysis of this phase using both wavelength and energy-dispersive

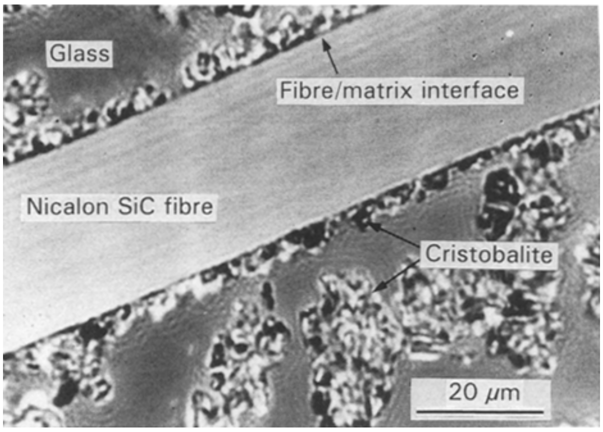

Figure 5 Scanning acoustic micrograph of a single-fibre 7740/SiC specimen showing formation of α-cristobalite along the fibre–matrix interface. $z = -1.0$ μm, imaging frequency = 1.9 GHz.

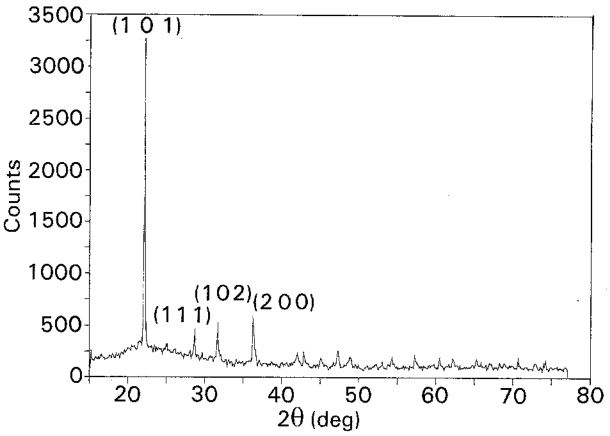

Figure 6 X-ray diffraction plot from a single-fibre 7740/SiC composite indicating the presence of α-cristobalite in the matrix.

spectrometers on a Camebax electron microprobe indicated that it was silicon rich (46 wt %), with no other heavy elements detected. Due to the requirement of a carbon coating for the specimen, the presence of elements lighter than carbon could not be determined. Analysis of the peaks in an X-ray diffraction (XRD) pattern obtained from the single-fibre specimen (Fig. 6) identified the crystalline phase as α-cristobalite, a tetragonal allotrope of silica which is metastable at room temperature. This agrees with previous results reported by Murty and Lewis [16] and subsequent workers [17, 18].

It has long been known that, despite being the high temperature (1470–1713 °C) silica phase, cristobalite can precipitate in borosilicate glass and remain metastable down to room temperature. Cox and Kirby [19] have linked the diffusion process controlling cristobalite-crystal growth to the removal of sodium and boron ions from the silicon–oxygen structure of the borosilicate glass, resulting in the formation of a crystalline region without any major positional changes of silicon and oxygen ions. More recently Clarke *et al.* [20] have investigated the formation of cristobalite in fabricated bulk hot-pressed borosilicate glass. The volume fraction of cristobalite in samples of borosilicate glass hot-pressed at temperatures in the range 750–950 °C was found to decrease with temperature but to increase with applied pressure.

As can be seen from the 0.45 V_f composite specimen (Fig. 2), cristobalite has formed at the fibre–matrix interface and also randomly throughout the borosilicate glass matrix. The volume fraction of cristobalite in the matrix was estimated at 0.4. In Fig. 5, cristobalite has intermittently precipitated at the fibre–matrix interface along its entire length. This has the effect of forming an *in-situ* coating approximately 3–5 μm thick along the fibre length. Comparing the volume fractions of cristobalite in the single fibre and high-fibre-volume-fraction composites, the presence of the fibres has given a comparatively small increase in the amount of cristobalite formed. In agreement with Bleay and Scott [18], these results indicate that nucleation of cristobalite at fibre surfaces is not the primary mechanism of matrix devitrification in 7740/SiC. Devitrification is most likely to occur at silica-rich regions of the glass [18, 20] or the surfaces of the powdered glass during hot pressing.

The fabrication of carbon-fibre-reinforced borosilicate is performed at temperatures of the order of 1200 °C [21–24]. Cristobalite is not observed to form in the matrix of the composite although Bleay and Scott [25] report the formation of small quantities of cristobalite at the fibre–matrix interface. The presence of a thin layer of cristobalite grains was also observed at the fibre–matrix interface in Corning-code-1723-aluminosilicate glass reinforced with Nicalon fibres. Murty *et al.* [26] have observed the same behaviour in 7740/SiC (incorporating both Nicalon and Tyranno fibres) fabricated at temperatures above the liquidus of borosilicate glass (~ 1100 °C). They concluded that at the more common hot-pressing temperature of ~ 950 °C matrix devitrification initiates at the surfaces of the powdered glass. As processing above the liquidus reduces these surfaces, the only mechanism enabling devitrification is precipitation at fibre–matrix interfaces.

The presence of cristobalite is detrimental to composite strength since cristobalite grains provide multiple stress concentrators. Hence the effective composite matrix microcracking stress will be lowered. However the profusion of partially debonded cristobalite–glass and cristobalite–fibre interfaces introduces a high volume fraction of interfaces, along which cracks preferentially propagate. Hence the composite is expected to be comparatively tough. This is supported by the high work of fracture which has been measured for this CMC system [2].

3.3. Matrix microcracking

The acoustic micrograph in Fig. 2 shows clearly the presence of extensive matrix microcracking. Matrix cracks are delineated by means of Rayleigh-wave-fringe formation (Fig. 7). These microcracks can be divided into three categories, which (i) connect neighbouring fibres, (ii) form around cristobalite grains and (iii) radiate out into the devitrified borosilicate-glass from the fibre–matrix interface. If large residual tensile

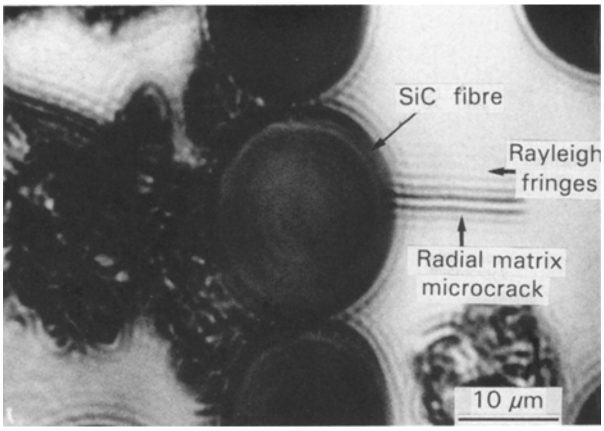

Figure 7 Scanning acoustic micrograph of 0.45 V_f 7740/SiC composite. $z = -2.0$ μm and the imaging frequency was 1.9 GHz. Note the radial microcrack in the devitrified glass matrix and cracks along the α-cristobalite/devitrified-interface highlighted by Rayleigh-wave-interference fringes.

radial thermal stresses were generated in the composite and the fibre–matrix interface had a comparatively low fracture toughness (an essential requirement for high composite fracture toughness) then fibre–matrix debonding should be observed using the SAM.

Examination of the composite using SEM (in secondary-electron and back-scattered modes) enabled matrix microcracking to be imaged (Figs 8 and 9). Whilst the contrast between fibres, glass and cristobalite is inferior to that obtained from SAM, the contrast from cracks is excellent. Of particular note is the propagation of cracks along the fibre–matrix interface (arrowed in Fig. 9). Fibre-matrix debonding (decohesion) is only visible where cristobalite grains are present at the interface. Thus fibre-matrix debonding appears to be associated with the precipitation and cooling of cristobalite to room temperature.

Although fibre-matrix debonding does not occur around the complete fibre circumference, it is still expected to affect composite properties. During tensile loading partially debonded fibres will begin to slide through the matrix at lower stresses than fully bonded fibres, the debonded regions acting as starter cracks over which frictional sliding can occur. Hence there will be a distribution of IFSS in the composite (the IFSS has been measured as 11.5–15.6 MPa with a standard deviation of approximately 7.0 MPa [26]). During tensile testing of the composite, there will be continuous fibre pull-out of broken fibres from the matrix at different composite stresses giving a high work of fracture. (Nicalon-silicon-carbide fibres exhibit a wide distribution in tensile strengths, σ_f (typically 0.7–2.8 GPa [28]). This results in progressive fibre failure and pull-out from the matrix. As the matrix fracture surfaces separate, the strength of the composite becomes determined by the remaining intact fibres. Composite ultimate tensile strength is thus the fracture strength of the fibre bundle, $V_f \sigma_f$.) Thus the composite will have a degree of damage tolerance, i.e. non-catastrophic pseudo-ductile failure. It is interesting to note that the other well characterized CMC system, LAS-III/SiC, also has a high work of fracture and low IFSS (with a mean of 4.2–8.3 MPa depending on the test method, with a standard deviation of approximately 4.0 MPa [27]) due primarily to partial circumferential fibre-matrix debonding [29, 30].

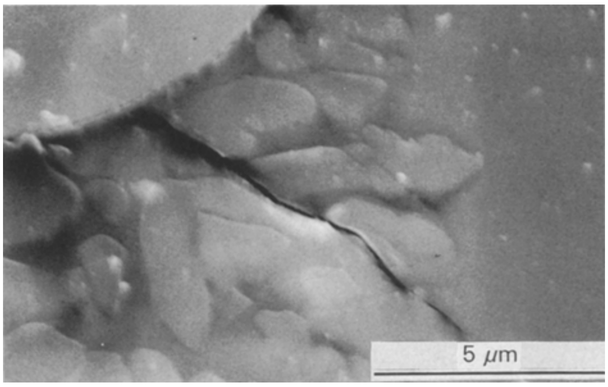

Figure 8 Secondary-electron micrograph showing matrix cracking around α-cristobalite particles.

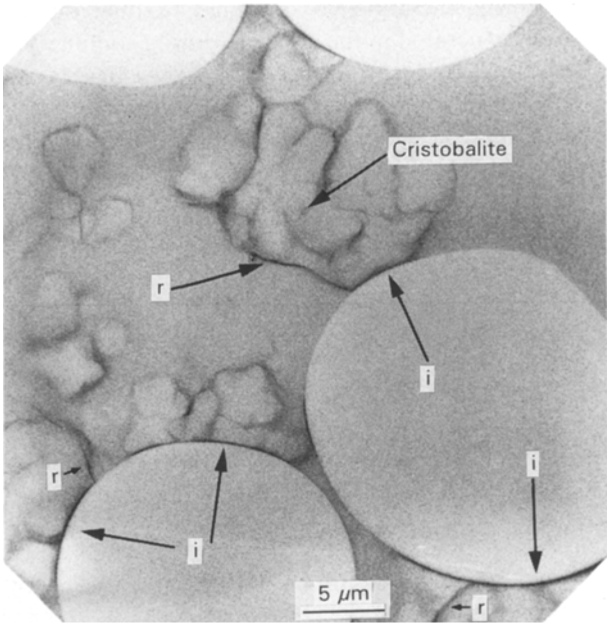

Figure 9 Back-scattered-electron micrograph of 7740/SiC. Arrows indicate cracks. Note the poor contrast from α-cristobalite, devitrified glass matrix and Nicalon-silicon-carbide fibres, and the excellent contrast from radial (r) and fibre–matrix interfacial (i) cracks.

In acoustic images such as Figs 2 and 7 it is not possible to observe directly the fibre-matrix bonding seen in the SEM, yet matrix microcracks are easily resolved. Due to the low ratio of fibre-to-matrix elastic modulus, the fibre–matrix interface in CMCs has a much lower impedance to acoustic waves than is the case for polymer matrix composites (PMCs). Hence only a small fraction (approximately 0.23 for 7740/SiC) of the acoustic power of Rayleigh waves incident on the fibre–matrix interface will be reflected back. i.e. the interface has a low reflection coefficient. Thus the Rayleigh-wave fringes formed on either side of the fibre–matrix interface are comparatively weak with respect to the background contrast. Debonding at the fibre–matrix interface results in the formation of a circumferential crack. As cracks have a comparatively high reflection coefficient much stronger fringes would be expected either side of a debonded interface (Reflection of Rayleigh waves from a crack has an associated phase change which will result in a shift of the fringe pattern by a fraction of the wavelength in the matrix). As fibre-matrix debonding is primarily associated with the presence of cristobalite in the matrix, it is difficult to observe fringe formation in the matrix side of the debond. In Fig. 7, variations in the fringe pattern around and within the fibres are just visible indicating partial fibre-matrix debonding has occurred around some of the fibres. The contrast across fibre–matrix interfaces in acoustic micrographs is discussed more fully in Part II [15].

Matrix microcracking has been observed in several other CMC systems (both glass and glass–ceramic [17]) being attributed to the high residual thermal stresses generated in the matrices during cooling from the processing temperatures (of the order of 1000 °C). These CMCs, however, had matrices which were essentially single phase, whereas for 7740/SiC the presence of cristobalite introduces a complicating factor. This leads us to expect that the matrix microcrack in Fig. 7 is a product of residual thermal stresses, whereas the microcracks associated with cristobalite grains are due to matrix devitrification. It can be concluded that at least two mechanisms contribute to matrix cracking in 7740/SiC: residual thermal stresses and matrix transformations.

4. Discussion

4.1. Matrix microcracking due to CTE mismatch between fibres and matrix

If the CTE of the reinforcing fibres differs from the matrix, then cooling the composite from hot-pressing to room temperature will result in thermal stresses being generated in both fibres and matrix. If the axial CTE of the fibres is lower than that of the matrix then the fibres will contract less than the matrix, and hence they will place the matrix in a state of tension which, if sufficiently great, may lead to a reduction in the composite's matrix cracking stress [31], or even spontaneous matrix microcracking. Conversely, if the axial CTE of the matrix is less than that of the fibres, the fibres will compress the matrix, effectively increasing the matrix microcracking strength of the composite when it is subjected to tensile loading. Residual radial and hoop thermal stresses in the composite can also affect composite tensile strength. Tensile radial thermal stresses across the fibre–matrix interface can result in fibre–matrix debonding, such behaviour has been observed in LAS-III/SiC [29] which can lead to a lower IFSS [31] and hence enhanced composite toughness [32]. High compressive thermal stresses across the fibre–matrix interface give rise to an increased IFSS resulting in a brittle material.

Various models have been produced to calculate the thermal stresses generated at room temperature by composite processing routes. The most realistic models assume a cylindrical geometry, with a thick coating of the matrix material surrounding the fibre [33]. Equations originally derived by Poritzky [34] have recently been used by Hegeler and Brückner [35] to investigate the influence of CTE mismatch on the mechanical properties of a series of Nicalon-reinforced glasses.

These equations allow the axial, radial and hoop (denoted by superscripts a, r, and h, respectively) thermal stresses to be determined in both the fibre (Equations 1–3) and matrix (Equations 4–6) of a composite as a function of radial distance from the fibre centre, r. The concise solutions used by Brugger [36] and Scherer [33] are employed.

$$\sigma_f^r = A\left(1 - \frac{b^2}{R^2}\right) \tag{1}$$

$$\sigma_f^h = A\left(1 - \frac{b^2}{R^2}\right) \tag{2}$$

$$\sigma_f^a = \sigma_m^a\left(1 - \frac{b^2}{R^2}\right) \tag{3}$$

$$\sigma_m^r = A\left(1 - \frac{b^2}{r^2}\right) \tag{4}$$

$$\sigma_m^h = A\left(1 + \frac{b^2}{r^2}\right) \tag{5}$$

$$\sigma_m^a = -\left(\frac{E_f E_m}{B - C}\right)\left(E_f(1 + \nu_m)\left(\frac{b^2}{R^2} + 1\right) + E_m(1 + \nu_f)\left(\frac{b^2}{R^2} - 1\right)\right)\int_{T_r}^{T_s}(\alpha_m - \alpha_f)\,\mathrm{d}T \tag{6}$$

where

$$A = -\left(\frac{E_f E_m}{B - C}\right)\left(E_f(1 + \nu_m) + E_m(1 + \nu_f)\left(\frac{b^2}{R^2} - 1\right)\right)\int_{T_r}^{T_s}(\alpha_m - \alpha_f)\,\mathrm{d}T \tag{7}$$

$$B = 2\left(E_f\nu_m + E_m\nu_f\left(\frac{b^2}{R^2} - 1\right)\right)^2 \tag{8}$$

$$C = \left(E_f\left(1 - \nu_m + (1 + \nu_m)\left(\frac{b^2}{R^2}\right)\right) + E_m(1 - \nu_f)\left(\frac{b^2}{R^2} - 1\right)\right) \times \left(E_f + E_m\left(\frac{b^2}{R^2} - 1\right)\right) \tag{9}$$

and E is Young's modulus, ν Poisson's ratio and the subscripts f and m refer to the fibre and matrix, respectively. α_m is the matrix CTE, and α_f the fibre CTE. T_r is room temperature and T_s the temperature at which stress relieving mechanisms cease to operate in the matrix. R is the fibre radius, b is the radius of the matrix layer (from the fibre centre) and r the radial distance in the matrix from the fibre centre.

The use of Equations 1–9 involves the following assumptions. First, that there is no interaction between the stresses around neighbouring fibres. This is reasonable for the axial thermal stress, but not for the radial and hoop thermal stresses. Secondly, the interstitial regions between the coated cylinders, of which the composite is assumed to consist, can be neglected (for a hexagonal array the interstitial regions comprise approximately 0.1 volume fraction of the entire composite volume). Hence to a first approximation, b^2/R^2 is the reciprocal of the fibre volume fraction. Thirdly, plane strain is assumed, which is a reasonable assumption for large length-to-diameter ratios (in practice, ratios of greater than three) [33]. Matrix viscoelastic effects are ignored.

When using the above equations, the temperature at which stress-relieving mechanisms cease to operate in the matrix, T_s, is needed. For crystalline matrices such as glass–ceramics, this can be considered to be the hot-pressing temperature (or the ceramming temperature, if a post-fabrication matrix-crystallization stage is used). In glass matrices, the hot-pressing temperature is near the liquidus, and the glass behaves as a viscous liquid and is thus able to flow in order to accommodate thermal stresses. For moderate cooling rates, the glass transition temperature, T_g (560 °C for borosilicate glass), is a reasonable value to use for T_s. Similarly, we need values for the fibre and matrix CTEs for temperatures up to the composite processing temperature. Typically, CTEs are only quoted as a mean linear value over a limited temperature range. However, as a consequence of the nature of interatomic bonding in solids, the CTE of a ceramic will only be linear for moderate temperatures. Ideally we require the CTE of both fibre and matrix as a function of temperature up to T_s. In practice the integral with respect to temperature of the CTE mismatch is assumed to be reasonably approximated by $(\alpha_m - \alpha_f)(T_s - T_r)$.

Taking CTE data reported by Hegeler and Brückner [35] and performing a linear fit, yields the following equation for the CTE temperature dependence of Nicalon

$$\alpha_f = 2.21 + 1.45 \times 10^{-3}\, T (10^{-6}\,°\mathrm{C}^{-1})$$

for $T = 200$–1300 °C. Unfortunately, the CTE for the borosilicate glass matrix is only known over the temperature range 20–300 °C, the mean value being $3.25 \times 10^{-6}\,°\mathrm{C}^{-1}$. Bearing these restrictions in mind, and using this data and the known elastic properties of the fibre (no experimentally measured value for Poisson's ratio of Nicalon-silicon-carbide fibres exists in the literature. Shetty [37], Faber *et al.* [38] and Hseuh *et al.* [39] all use a value of 0.15, but do not give a reference for the source. Bulk α-silicon-carbide has a Poisson's ratio of 0.19 [35]) and matrix (Table I), the residual thermal stresses can be estimated in the borosilicate-glass matrix at room temperature. Inserting values in Equations 4–6 yields: $\sigma^a_m = 13$ MPa, $\sigma^r_m = -8$ MPa (negative values indicate compressive stress) and $\sigma^h_m = 18$ MPa. The calculated thermal stresses in the fibres are $\sigma^a_f = -19$ MPa, $\sigma^r_f = -8$ MPa and $\sigma^h_f = -8$ MPa[4]. The *in-situ* tensile strengths of the fibres are significantly greater than those of the matrix (approximately 1.5 GPa and 50 MPa respectively), hence the possibility of fibre fracture can be neglected. Thus discussion will be confined to thermal stresses generated in the matrix. As can be seen from Equations 4 and 5 the radial and hoop thermal stresses decay radially in the matrix. The maximum value has been calculated for these stresses generated in the matrix, i.e. when $r = R$. These stresses are well below the tensile strength of monolithic borosilicate glass (48 MPa) and the composite matrix microcracking stress (approximately 275 MPa). Hence they are unlikely to be responsible for the matrix microcracking visible in Figs 2, 8 and 9.

Hegeler and Brückner [35] have investigated the influence of thermal expansion on the strength and fracture toughness of a range of glass-matrix composites. They found that whilst some systems generated tensile thermal stresses greater than the tensile strengths of the bulk matrix glass, matrix microcracking was not observed. They concluded that the higher strengths associated with glass fibres (> 1.0 GPa) or thin films were a more appropriate comparison than bulk-glass tensile strength and that the fibre–matrix interfaces in the CMCs examined were free from defects. If true, this would support our conclusion that fibre-matrix CTE mismatch does not give rise to matrix microcracking in 7740/SiC. Note however, that matrix microcracking has been observed in a range of glass and glass–ceramic matrix composites and was found to correlate with high residual thermal stresses [17].

4.2. Matrix microcracking due to CTE mismatch between cristobalite and matrix

Just as the CTE mismatch between the Nicalon fibres and glass matrix gives rise to residual thermal stresses, so will that between the cristobalite and the devitrified glass matrix. Analysis of these stresses is complicated by the β-to-α-cristobalite phase change. Equations exist which enable the radial and hoop thermal stresses in the matrix (σ^r_m and σ^h_m, respectively) to be determined [41, 42] (since spherical geometry and an isotropic matrix are assumed only radial and tangential stresses have to be considered). For an elastic matrix, these equations are [33, 43]

$$\sigma^r_m = D\left[\left(\frac{R}{r}\right)^3 - \left(\frac{R}{b}\right)^3\right] \tag{10}$$

$$\sigma^h_m = -D\left(\frac{1}{2}\left(\frac{R}{r}\right)^3 + \left(\frac{R}{b}\right)^3\right) \tag{11}$$

$$D = \left(\frac{2E_m}{3(1-\nu_m)}\right) \times \left(\frac{\int_T^{T_s} (\alpha_m - \alpha_p)\,\mathrm{d}T}{1 - (1 - K_m/K_p)(1 - V_p)(1 - \beta)}\right) \tag{12}$$

where α_p, ν_p, and E_p are the CTE, Poisson's ratio and Young's modulus of the particle. $V_p = (a/b)^3$ is the particle volume fraction, $K = E/3(1 - 2\nu)$ is the bulk modulus and $\beta = (1 + \nu_m)/3(1 - \nu_m)$.

As with the fibre-matrix case, the use of Equations 10–12 is limited by knowledge of the appropriate

TABLE II Calculated residual stresses in glass-matrix composites due to processing conditions

Phases causing residual stress	ΔT (°C)	α_m (10^{-6} °C^{-1})	$\alpha_{f,p}$ (10^{-6} °C^{-1})	E_m (GPa)	$E_{f,p}$ (GPa)	σ_a (MPa)	σ_r (MPa)	σ_h (MPa)
1723-glass/SiC	690	4.58	3.24	94	205	84	− 49	115
7740-glass/SiC	540	3.25	3.02	93	205	13	− 8	18
7740-glass/β-cristobalite	315	3.25	27.1	93	70[a]	239	239	− 359
β/α phase change	–	–	–	93	70[a]	–	2200	–
7740-glass/α-cristobalite	225	3.25	50.0	63	70[a]	335	335	− 503

[a] The modulus of both cristobalite phases is assumed to be approximately identical to fused silica.

material properties. Estimates of the thermal stresses can be made if it is assumed that the elastic properties of both α- and β-cristobalite are effectively indistinguishable from the devitrified glass, which in turn has identical properties to the intial borosilicate–glass matrix. On cooling the composite, cristobalite will exist in the β-form until 220–270 °C (see Section 4.3). MacMillan [44] quotes the CTE of cristobalite as 27.1×10^{-6} °C^{-1} for $T = 20$–600 °C and 50.0 $\times 10^{-6}$ °C^{-1} for $T = 20$–300 °C. Assuming that at the higher temperature the β-phase dominates the measured CTE and that at the lower temperature the α-phase dominates, then these values can be used to estimate the corresponding stresses. Inserting values gives: $\sigma_r = 239$ MPa and $\sigma_h = -359$ MPa; for $T = 245$–560 °C; and $\sigma_r = 335$ MPa and $\sigma_h = -503$ MPa, for $T = 20$–245 °C.

The radial thermal stresses calculated for the CTE mismatch between both α- and β-cristobalite grains and the devitrified glass are similar to the expected cristobalite-glass bond strength (see Section 4.3). Hence cracking/debonding of the cristobalite–glass interface is probable. Thermal hoop stresses generated in the matrix are compressive for both α- and β-cristobalite grains and thus oppose the formation of radial matrix microcracks. These calculations thus indicate that the high CTE of α- and β-cristobalite gives rise to the observed matrix cracking in 7740/SiC. As β-cristobalite is the higher-temperature allotrope of silica, it is this phase which will give rise to the cracking seen at room temperature.

4.3. Matrix microcracking due to phase transformation

Above 230 °C (the precise temperature at which β-cristobalite transforms to α-cristobalite is dependent on the initial purity of the β-cristobalite, ranging from 220–270 °C [40]), cristobalite exists in the β-form; however, on cooling through 230 °C it undergoes a martensitic phase change from β- to α-cristobalite with an associated volume decrease of 5.7%. As the α-cristobalite shrinks away from the glass matrix, tensile stresses will be generated across the cristobalite–borosilicate-glass interface. If sufficiently high, this will lead to particle debonding and possibly crack growth in the glass phase. The critical stress, σ_d, for particle/glass debonding can be estimated using an energy-balance approach. The strain energy released as the particle undergoes the β/α phase change is assumed to be balanced by the creation of interfacial fracture surfaces and hence surface energy. Nucleation of an interfacial debond crack is not considered. Thus the following expression is obtained [41]

$$\sigma_d \geqslant \left(\frac{8\varphi\gamma_i}{(1 + \nu_m)/E_m + 2(1 - 2\nu_p)/E_p} \left(\frac{1}{R}\right) \right)^{1/2} \tag{13}$$

where γ_i is the effective fracture energy per unit area of the α-cristobalite–devitrified-glass-matrix interface. R is the radius of the α-cristobalite grain, E_m and E_p are the Young's modulus of the matrix and particle respectively, φ is the fraction of the interface which debonds. We do not know the fracture energy of the α-cristobalite–devitrified-glass interface, although we can assume a lower limit equal to that of borosilicate glass, 10 J m^{-2}. Taking the mean particle radius to be 3 μm and using the appropriate material properties from Table II, Equation 13 predicts a lower-bound critical stress for complete particle/glass debonding of approximately $940\varphi^{1/2}$ MPa. The fraction of the interface debonded varied from particle to particle, but the assumption of an average value for φ of 0.2–0.3 predicts a bond strength of 420–515 MPa. As the interface is non-planar the effective fracture energy of the interfacial crack would be expected to be much higher, and hence the critical debond stress would be expected to be greater than predicted using this simple model.

In order to calculate the actual stress generated during the β/α cristobalite phase change, it is assumed that the cristobalite grains are spherical and have the same elastic properties as the glass matrix. The tensile stress across the cristobalite–glass interface due to the volume change (dilatation) associated with the β/α cristobalite phase, $\sigma_{\beta/\alpha}$, can then be calculated approximately using the simple relationship:

$$\sigma_{\beta/\alpha} = \frac{-E_p\Delta}{3(1 - 2\nu_p)} \tag{14}$$

where Δ is the volume change and E_p and ν_p the Young's modulus and Poisson's ratio of the particle respectively. Inserting the appropriate values in Equation 14 the tensile stress across the cristobalite–glass interface is estimated to be 2.2 GPa, two orders of magnitude greater than the thermal stresses generated due to the CTE mismatch between the fibres and matrix. It can be concluded that cracking in the glass matrix of 7740/SiC is not a result of the CTE mismatch between cristobalite (either β or α) and the devitrified glass, but is primarily due to the volume decrease associated with the β/α phase change. Note that as the β/α-cristobalite phase transition involves a volume *decrease*, any hoop stress generated in the glass matrix will be compressive and thus restrict radial-crack nucleation and growth. Additional stresses will be present in the matrix due to the CTE mismatch between cristobalite and the devitrified matrix, but, as shown in Section 4.2, these are significantly lower than that due to the β/α phase change. The high stress developed due to the β/α phase change explains the observation that fibre-matrix debonding only occurred along the cristobalite–fibre interface and suggests that the interface in 7740/SiC has a comparatively high work of fracture. Table II tabulates the stresses induced in the matrix of 7740/SiC by thermal expansion mismatches and phase transformations during composite fabrication.

Note from micrographs such as Figs 7–9 that complete particle debonding seldom occurs and that some cracks terminate in the devitrified glass matrix. As Equation 13 is only a lower bound for the debond stress, it is likely that the interface between cristobalite and the glass is much stronger than calculated. A further restriction of Equation 13 is the absence of data for the elastic properties of cristobalite and the devitrified glass matrix. As the particles deviate from the assumed spherical symmetry, the stresses generated across the cristobalite–glass interface will vary, debonding then occurring at the points of maximum stress. The irregular shape of the cristobalite particles may well be the cause of the few instances of observed crack growth into the devitrified glass. Micrographs such as Figs 8 and 9 show that crack surface separation can be quite large around cristobalite particles, supporting the calculation of large matrix stresses. Cracks in the matrices of other CMC systems due to fibre/matrix CTE mismatch were found to have very little crack opening [17].

5. Conclusions

The SAM is able to produce high-contrast images of composite microstructures enabling matrix defects to be identified without the requirement for a conductive coating.

2. The formation of Rayleigh-wave fringes both within and around the fibres allows the *in-situ* elastic properties of the fibres and matrix to be estimated. These properties may in turn contribute to an account of the cracks observed in the matrix.

3. The matrix of Nicalon-reinforced-borosilicate glass experienced considerable devitrification resulting in the random distribution of cristobalite throughout the matrix. Although present at the fibre–matrix interface, precipitation was not found to be the most significant source of cristobalite nucleation under the given composite-processing conditions.

4. The matrix was found to be extensively microcracked. In areas of high concentrations of fibres and cristobalite these cracks joined neighbouring fibres forming a complex three-dimensional network of defects.

5. Calculations of the thermal stresses induced in the matrix due to the CTE mismatch between fibre and matrix indicated that this was unlikely to explain the observed matrix microcracking.

6. The thermal stresses due to CTE mismatch between α- and β-cristobalite and the devitrified borosilicate glass were found to be of the same order of magnitude as the calculated debond stress. Hence cracking may occur around cristobalite particles due to these thermal stresses. As β-cristobalite is the high-temperature form, it is this phase which gives rise to the observed matrix microcracking at room temperature.

7. Simple calculations indicated that matrix microcracking is more likely to be due to the very high stresses associated with the contraction when β-cristobalite transforms to α-cristobalite at 220–70 °C. These stresses are sufficient to cause cristobalite/glass and cristobalite/fibre debonding and they also increase with decreasing particle size.

8. The formation of cristobalite in the matrix of 7740/SiC causes some degradation of the composite matrix microcracking stress, but also results in improved fracture toughness compared with single-phase matrices, due to the proliferation of energy-absorbing interfaces.

9. Nicalon-reinforced borosilicate glass fabricated under notionally optimum conditions cannot be considered as a simple fibre/single-phase matrix system. The formation of a crystalline phase in the original glass matrix requires the final composite matrix to be modelled as a glass–ceramic with a high residual glass content rather than a single isotropic ceramic phase.

Acknowledgements

The authors thank Dr P. M. Mummery and Mr C. Salter for their assistance with electron microscopy and microanalysis and Dr B. Derby for his stimulating discussions. CWL was funded by a SERC studentship.

References

1. D. C. PHILIPS, *J. Mater. Sci.* **7** (1972) 1175–1191.
2. D. M. DAWSON, R. F. PRESTON and A. PURSER, *Ceram. Engng Sci. Proc.* **8** (1987) 815–22.
3. R. W. DAVIDGE and J. J. R. DAVIES, *Int. J. High. Tech. Ceram.* **4** (1988) 341–58.
4. T. MAH, M. MENDIRATTA, A. KATZ, R. RUH and K. MAZ DIGASNI, *J. Amer. Ceram. Soc.* **68** (1985) C 248.
5. A. F. FAGAN, G. A. D. BRIGGS, J. T. CZERNUSZKA and C. B. SCRUBY, *J. Mater. Sci.* **27** (1992) 1202–1206.
6. D. G. P. FATKIN, C. B. SCRUBY and G. A. D. BRIGGS, *J. Mater. Sci.* **24** (1989) 23–40.
7. C. B. SCRUBY, C. W. LAWRENCE, D. G. P. FATKIN, G. A. D. BRIGGS, A. DUNHILL, A. E. GEE and C-L. CHAO, *Brit. Ceram. Trans. J.* **88** (1989) 127–32.
8. K. YAMANAKA and Y. ENOMOTO, *J. Appl. Phys.* **53** (1982) 846–50.
9. G. A. D. BRIGGS, P. J. JENKINS and M. HOPPE, *J. Microscopy* **159** (1990) 15–32.
10. K. CHYUNG, Private communication, August, 1989.
11. Nicalon silicon carbide fibre data sheet, Nippon Carbon Company.
12. A. SEERAT UN NABI and B. DERBY, *J. Mater. Sci. Lett.* **9** (1990) 63–66.
13. D. H. GRANDE, J. F. MANDELL and K. C. C. HONG, *J. Mater. Sci.* **23** (1988) 311–28.
14. A. BRIGGS and R. W. DAVIDGE, *Mater. Sci. Engng A* **109** (1989) 363–72.

15. C. W. LAWRENCE, G. A. D. BRIGGS and C. B. SCRUBY, *J. Mater. Sci.* **28** (1993) 3645.
16. V. S. R. MURTY and M. H. LEWIS, *J. Mater. Sci. Lett.* **8** (1989) 571–72.
17. C. W. LAWRENCE, C. B. SCRUBY and G. A. D. BRIGGS, *Inst. Phys. Conf. Ser. No 98* (1990) 139–42.
18. S. M. BLEAY and V. D. SCOTT, *J. Mater. Sci.* **26** (1991) 2229–39.
19. S. M. COX and P. L. KIRBY, *Nature*, **159** (1947) 162–3.
20. S. G. CLARKE, S. M. BLEAY and V. D. SCOTT, *J. Mater. Sci. Letts.* **10** (1991) 149–53.
21. D. C. PHILIPS, *J. Mater. Sci.* **7** (1972) 1175–91.
22. D. C. PHILIPS, *J. Mater. Sci.* **9** (1974) 1847–54.
23. K. M. PREWO, *J. Mater. Sci.* **23** (1988) 2745–52.
24. D. C. PHILIPS, R. A. J. SAMBELL and D. H. BOWEN, *J. Mater. Sci.* **7** (1972) 1454–64.
25. S. M. BLEAY and V. D. SCOTT, *J. Mater. Sci.* **26** (1991) 3544–52.
26. V. S. R. MURTY, M. W. PHARAOH and M. H. LEWIS, *Material Lett.* **10** (1990) 161–4.
27. C. W. LAWRENCE, S. KOONER, T. P. WEIHS and B. DERBY, in "Interfacial phenomena in composite materials '91", edited by I. Verpoest and F. Jones, (Butterworth-Heinemann, Oxford, 1991) pp. 208–11.
28. L. C. SAWYER, R. ARONS, J. B. STUNADOFF and J. RABE, *Ceram. Engng Sci. Proc.* **6** (1985) 567–75.
29. R. CHAIM and A. H. HEUER, *Adv. Ceram. Mats.* **2** (1987) 154–58.
30. T. P. WEIHS and W. D. NIX, *J. Amer. Ceram. Soc.* **74** (1991) 524–34.
31. B. BUDIANSKY, J. W. HUTCHINSON and A. G. EVANS,. *J. Mech. Phys. Solids* **34** (1986) 167–89.
32. T. P. WEIHS, O. SBAIZERO, E. Y. LUH and W. D. NIX, *J. Amer. Ceram. Soc.* **74** (1991) 535–40.
33. G. W. SCHERER, in "Relaxation in glass and composites" (John Wiley & Sons, New York, 1986).
34. H. PORITSKY, *Phys.* **5** (1934) 406–11.
35. H. HEGELER and R. BRÜCKNER, *J. Mater. Sci.* **25** (1990) 4836–46.
36. K. BRUGGER, *Appl. Optics* **10** (1971) 437–8.
37. D. K. SHETTY, *J. Amer. Ceram. Soc. C* **71** (1988) 107–8.
38. K. T. FABER,. S. H. ADVANI, J. K. LEE and J. T. JINN, *J. Amer. Ceram. Soc. C* **69** (1986) 208–9.
39. C-H. HSUEH, M. K. FABER and P. F. BECHER, *J. Mater. Res.* **4** (1989) 1529–37.
40. Ceramic Source, Vol. 5, (The American Ceramic Society, OH, 1989) p. 315.
41. R. W. DAVIDGE and T. J. GREEN, *J. Mater. Sci.* **3** (1968) 629–34.
42. V. D. KRISTIC and M. D. VLAJIC, *Acta. Metall.* **31** (1983) 139–44.
43. G. W. SCHERER *J. Amer. Ceram. Soc.* **66** (1983) 59–65.
44. P. W. McMILLAN, in "Glass Ceramics" (Academic Press, London, 1964) pp. 132–57.

Received 11 September
and accepted 10 December 1992